Published in final edited form as:
Biochemistry. 2007 October 23; 46(42): 11969–11978. doi:10.1021/bi700925n.

Characterization of Alkyl-Nickel Adducts Generated by Reaction of Methyl-Coenzyme M Reductase with Brominated Acids

Mishtu Dey[‡], **Ryan C. Kunz**[‡], **Derek M. Lyons**[§], and **Stephen W. Ragsdale**[‡,*]

[‡]Department of Biochemistry, University of Nebraska, Lincoln, NE 68588

[§]Simpson College, Indianola, IA 50125

Abstract

Methyl-coenzyme M reductase (MCR) from methanogenic archaea catalyzes the final step in the biological synthesis of methane. Using coenzyme B (CoBSH) as the two-electron donor, MCR reduces methyl-coenzyme M (methyl-SCoM) to methane and the mixed disulfide, CoB-S-S-CoM. MCR contains Coenzyme F_{430}, an essential redox-active nickel tetrahydrocorphin at its active site. The active form of MCR (MCR_{red1}) contains Ni(I)-F_{430}. When 3-bromopropane sulfonate (BPS) is incubated with MCR_{red1}, an alkyl-Ni(III) species is formed that elicits the MCR_{PS} EPR signal. Here we used EPR and UV-visible spectroscopy and transient kinetics to study the reaction between MCR from *Methanothermobacter marburgensis* and a series of brominated carboxylic acids, with chain lengths from 4 to 16 carbons long. All of these compounds give rise to an alkyl-Ni intermediate with an EPR signal similar to that of the MCR_{PS} species. Reaction of the alkyl-Ni(III) adduct, formed from brominated acids with 8 or less total carbons, with HSCoM as nucleophile at pH 10.0 results in the formation of a thioether coupled to regeneration of the active MCR_{red1} state. When reacted with 4-bromobutyrate, MCR_{red1} forms the alkyl-Ni(III) MCR_{XA} state and then, surprisingly, undergoes "self-reactivation" to regenerate the Ni(I) MCR_{red1} state and a bromocarboxy ester. The results demonstrate an unexpected reactivity and flexibility of the MCR active site to accommodate a broad range of substrates, which act as molecular rulers for the substrate channel in MCR.

Methanogenic archaea are anaerobic microbes that form methane as an end product of their metabolism. Methanogens produce approximately 1 billion tons of methane every year, providing a valuable source of renewal energy. On the other hand, methane is a greenhouse gas that is 20 times more potent than CO_2 and therefore poses potential environmental problems (1). Methyl coenzyme M reductase (MCR), found in all methanogens, is a nickel containing enzyme that catalyzes the terminal step in biological methane formation, which is the reduction of methyl-coenzyme M (2-(methylthiol)ethane sulfonate, methyl-SCoM) with the two-electron donor coenzyme B, (N-7-mercaptoheptanolyl-threonine phosphate, CoBSH), to form methane and the heterodisulfide CoBS-SCoM (1-3). There is strong evidence that MCR or a MCR-like enzyme also catalyzes the first step in the anaerobic oxidation of methane (4). The active site of MCR contains a redox-active Ni-tetrapyrrolic cofactor called coenzyme F_{430} (or simply F_{430}) that is thought to play an essential role in catalysis (5-7). The crystal structure(s) of MCR reveals that F_{430} is non-covalently bound to

[*]CORRESPONDING AUTHOR CONTACT INFORMATION: Phone: 402-472-2943; FAX: 402-472- 4961; sragsdale1@unl.edu
AFTER AUG 1, 2007: Phone: (734) 763-6459; FAX: (734) 764-3509; sragsdal@umich.edu.
After Aug 1, all authors will be at this address: Department of Biological Chemistry, MSRB III, 5301, 1150 W. Medical Center Drive, Ann Arbor, MI 48109-0606

Supporting Information Available. Eight figures showing second order rate constant determination for the formation of various MCR_{XA} complexes. This material is available free of charge via the Internet at http://pubs.acs.org

MCR and sits at the bottom of a 30 Å hydrophobic channel (8) that is sufficiently deep to accommodate both substrates.

The Ni atom of F_{430} in MCR can exist in 3 different oxidation states, each exhibiting several coordination states. Active MCR_{red1} contains Ni(I), which is the form that can react with methyl-SCoM to catalyze methane formation (9, 10). In addition to MCR_{red1}, two other states of MCR that could be relevant for the catalytic mechanism are MCR_{ox1} and MCR_{PS}.

Based on spectroscopic and computational studies, MCR_{ox1} is best described as a high spin Ni(II)/thiyl-radical that is in resonance with a Ni(III)/thiolate species (11, 12). MCR_{ox1} resembles a proposed catalytic intermediate and is called the "ready state" (9) because it can be converted to MCR_{red1} *in vitro* by incubation with the low potential reductant, titanium(III) citrate (Ti(III) citrate) (10). MCR_{ox1} is generated *in vivo* by treating the actively growing cells with sodium sulfide (13) or alternatively, by switching the gas from 80%H_2/20%CO_2 to 80%N_2/20%CO_2 (14). MCR_{ox1} can be generated *in vitro* by treating MCR_{red2} (MCR_{red1} in the presence of HSCoM and CoBSH) with polysulfide (15).

The second state of MCR that may be relevant for catalysis is MCR_{PS} (formerly MCR_{BPS}) (16). MCR_{PS} has been described as a high-spin Ni(II)/alkylsulfonate radical species resonating with a Ni(III)/alkyl species (17, 18), and, thus, resembles the proposed methyl-Ni catalytic intermediate. MCR_{PS} is generated *in vitro* by incubating MCR_{red1} with 3-bromopropane sulfonate (BPS) (16), which is a potent inhibitor (apparent K_i = 50 nM) (19, 20) of MCR that also has been classed as an irreversible inhibitor (21). However, when it was recognized that the MCR_{PS} state can be converted back to the active MCR_{red1} state by reacting with thiolates, reversing inhibition, BPS was classified as a reversible redox inactivator (22). Thus, both MCR_{PS} and MCR_{ox1} are "ready" states that can generate MCR_{red1} *in vitro*; furthermore, they exhibit similar UV-visible and EPR spectra.

The two mechanisms for methane formation can be distinguished by the first step of catalysis (**Figure 1**). In Mechanism I, which is based on the crystal structure and mechanistic work with F_{430} model complexes (23-25), nucleophilic attack of Ni(I)-MCR_{red1} on the methyl group of methyl-SCoM generates a methyl-Ni intermediate (26). Although a true methyl-Ni intermediate has not been described upon reaction of MCR_{red1} with the native substrate methyl-SCoM, the reaction of BPS and other alkyl halides with MCR_{red1} generates an alkyl-Ni(III) species that is subsequently attacked by free organic thiolates to generate the thioether product and MCR_{red1} (22). This reaction is analogous to that of the reaction catalyzed by methionine synthase, where homocysteine acts as a nucleophile to reduce methyl-Co(III) to form Co(I) and methionine (27).

Mechanism II, which is based on density function theory computations (28, 29), avoids the methyl-Ni(III) species because cleavage of the strong methyl-S bond of methyl-SCoM to form a relatively weak methyl-Ni(III) species was calculated to be extremely endothermic (45 kcal/mol). Therefore, Mechanism II proposes attack of Ni(I) on the sulfur atom adjacent to the methyl group of methyl-SCoM resulting in homolytic cleavage of the methyl-sulfur bond to generate a methyl radical and a Ni(III)-thiolate/Ni(II)-thiol-radical complex (MCR_{ox1}-like species) (**Figure 1**).

It was recently shown (22) that the alkyl-Ni(III) species (MCR_{PS}) can be converted to the active MCR_{red1} state when it is reacted with various thiols at pH 10.0. The MCR_{PS} intermediate is chemically similar to the proposed alkyl-Ni intermediate in the first step of Mechanism I; however, the position of attack on BPS is stereochemically comparable to the first step in Mechanism II. The position of attack by Ni(I) is probably influenced by the placement of BPS (or other analogs) in the active site. Based on the $MCR_{ox1\text{-}silent}$ crystal

structure, the sulfonate group of HSCoM is firmly anchored by three contacts at the “back” of the active site and the thiolate is ligated to Ni. Similarly, the reactivity of CoBSH would be influenced by its location in the substrate channel relative to the position of the Ni-bound ligand. CoBSH has phosphate and carboxylate groups that anchor it to the upper lip of the channel and an alkyl chain that leads into the active site and terminates in a thiol group 8.7 Å from the nickel atom of F_{430} (8).

In order to better understand the selectivity of the MCR reaction toward nucleophilic attack by Ni(I), one could compare the reactivity of a series of brominated sulfonates of varying chain length. However, such a series of compounds is not commercially available. On the other hand, substitution of the sulfonate of BPS with a carboxylate still allows formation of a MCR_{PS}-like signal (22), which we call MCR_{XA}. Furthermore, methylmercaptopropionate is a substrate for MCR ($k_{cat}/K_M = 26\ M^{-1}\ s^{-1}$), albeit ~ 110-fold less reactive than the natural substrate, methyl-SCoM ($k_{cat}/K_M = 2.8 \times 10^3\ M^{-1}s^{-1}$) (30), and bromopropionate (like BPS) is an inhibitor (18), indicating that brominated carboxylic acids mimic the interactions of BPS and methyl-SCoM at the MCR active site. Therefore, in order to better understand the selectivity of the MCR reaction, we have in this paper compared the reactivity of a series of brominated compounds of varying chain lengths in formation of the alkyl-Ni(III) complexes and in the subsequent reaction with organic thiol to regenerate the active enzyme.

Here we show that various brominated acids ranging from the relatively small bromobutyric acid (Br4A) to the relatively large bromohexadecanoic acid (Br16A) can all react with MCR_{red1} to form an EPR-active species, MCR_{XA}, that is nearly identical to MCR_{PS}. Based on the present studies a model has been proposed for the mode of binding of various brominated acids of different chain lengths that can be classified as: (a) methyl-SCoM-like and (b) CoBSH-like. The results provide information on the selectivity of MCR for its substrates (methyl-SCoM, CoBSH and BPS) and may aid in the development of other substrate analogs or inhibitors of MCR.

Materials and Methods

Materials and Organism

Methanothermobacter marburgensis (f. *Methanobacterium thermoauotrophicum* strain Marburg) was obtained from the Oregon Collection of Methanogens (Portland, OR) catalogue as OCM82. All buffers, media ingredients, and other reagents were acquired from Sigma-Aldrich (St. Louis, MO) unless otherwise stated and were of the highest purity available. Solutions were prepared using Nanopure deionized water. N_2 (99.98%), H_2S (99.0 %), H_2/CO_2 (80%/20%), and Ultra High Purity (UHP) H_2 (99.999%) were obtained from Linweld (Lincoln, NE). Ti(III) citrate solutions were prepared from a stock solution of 200 mM Ti(III) citrate, which was synthesized by adding an aqueous solution of sodium citrate (5.8 g sodium citrate added to 20 ml H_2O) to Ti(III) trichloride (30 weight % solution in 2 M hydrochloric acid) (Acros Organics, Morris Plains, NJ) under anaerobic conditions and adjusting the pH to 7.0 with a saturated solution of sodium bicarbonate (31). The concentration of Ti(III) citrate was determined routinely by titrating a methyl viologen solution.

M. marburgensis growth, harvest and MCR_{red1} purification conditions

MCR_{red1} was isolated from *M. marburgensis* cultured on $H_2/CO_2/H_2S$ (80%/20%/0.1%) at 65 °C in a 14-L fermentor (New Brunswick Scientific Co., Inc. New Brunswick, NJ) (9). Culture media were prepared as previously described (32). MCR_{red1} was generated *in vivo* and purified as described earlier (22). The purification procedure routinely generates 60-70 % MCR_{red1} as determined by UV-visible and EPR spectroscopy described earlier (22)

Spectroscopy of MCR

UV-visible spectra of MCR were recorded in the anaerobic chamber using a diode array spectrophotometer (Model DT 1000A, Analytical Instrument Systems, Inc., Flemingron, NJ). EPR spectra were recorded on a Bruker EMX spectrometer (Bruker Biospin Corp., Billerica, MA), equipped with an Oxford ITC4 temperature controller, a Hewlett-Packard Model 5340 automatic frequency counter and Bruker gaussmeter. Unless otherwise noted, the EPR spectral parameters included: temperature, 70 K; microwave power, 10 mW; microwave frequency, 9.43 GHz; receiver gain, 2×10^4; modulation amplitude, 10.0 G; modulation frequency, 100 kHz. Double integrations of the EPR spectra were performed and referenced to a 1 mM copper perchlorate standard.

Stopped-Flow Studies

Stopped-flow experiments were carried on an Applied Photophysics spectrophotometer (SX.MV18, Leatherhead, UK) equipped with a photodiode array detector. Rigorous measures were taken to remove oxygen from the stopped-flow instrument. Buffered solutions of enzymes and inhibitors were made in the anaerobic chamber in 0.5 M Tris-HCl, pH 7.6 containing 0.2 mM Ti(III) citrate at 25 °C. All buffered solutions contained 0.2 mM Ti(III) citrate as an oxygen scavenger, since exclusion of Ti(III) citrate resulted in oxidation of MCR_{red1}. The solutions were then loaded into tonometers, which had been incubated in the anaerobic chamber for at least 4 days and served as reservoirs for the drive syringes of the stopped-flow instrument. The drive syringes and mixing chamber were made anaerobic by flushing the syringe chamber with a dithionite:resazurin (1 mM: 0.02 mM) solution in 0.1M NaOH. MCR_{red1} and varied concentrations of brominated acids were rapidly mixed at 25 °C in a 1:1 ratio. The reaction was monitored in the single wavelength mode by following the decrease of MCR_{red1} at 385 nm and MCR_{XA} formation was followed at 420 nm, with a 1 cm pathlength. Data were fit to a single exponential decay and exponential rise to maximum functions, respectively, using software provided by Applied Photophysics (version SX MV.18) or using Sigma Plot 2001 (Point Richmond, CA). Reported rate constants are the average of at least three different rapid-mixing experiments.

Mass spectromety

All mass spectra (LCMS) were collected in negative ion modes by direct infusion to a [4000 Qtrap (ABS)] mass spectrometer using a kD Scientific micro flow syringe pump. The data was acquired and processed using Analyst 1.4.1 software. Data was acquired in Q1 (quadrupole one) and Product ion scan in negative ion mode. The mass range of 50-300 amu (atomic mass units) was scanned in 1s. The ionspray voltage was set to -4500 V, the temperature was set to 22 °C and a declustering potential (DP) value was -50 V. MCR_{red1} (10 μM) was incubated for 10 min with 2.0 mM 4-bromobutyric acid (Br4A was prepared as a stock solution in 0.1 M formic acid; thus, the final concentration of formic acid in the reaction mixture is 0.4 mM) in 20 mM ammonium carbonate, pH 10.0, and the reaction was followed by UV-visible spectroscopy. For, the regeneration of MCR_{red1} from MCR_{XA} with HSCoM, typically 20 μM MCR_{red1} was reacted with 1 mM brominated acid in 50 mM ammonium carbonate, pH 10 to form MCR_{XA}, which was then reacted with 20 mM HSCoM. This reaction was monitored by UV-visible spectroscopy. After MCR_{red1} was fully reactivated, assessed by reaching a stable maximum absorbance of the 385 nm band, the reaction was stopped by freezing in liquid nitrogen. For analysis, the frozen liquid was thawed and, subsequently, enzyme and ligands were separated using a 0.5 mL Microcon centrifugal filter device with a 30 KDa cut-off filter (Millipore, Billerica, MA). The filtrate containing the product was collected and stored at 4 °C until it was assayed by mass spectrometry. All MS samples were prepared by mixing the ligand solution with an equal volume of acetonitrile.

Reactions between MCR_{red1} and brominated acids

MCR_{red1} (typically 0.01-0.02 mM) was incubated in 50 mM Tris-HCl (pH 7.6) at 25 °C for 0.5-2 min, with various brominated acids at concentrations between 0.1 mM and 2 mM: 0.2 mM 4-bromobutyric acid (Br4A) in 0.1 mM final formic acid concentration, 0.2 mM 5-bromovaleric acid (Br5A), 0.2 mM 6-bromohexanoic acid (Br6A), 1.0 mM 7-bromoheptanoic acid (Br7A) (Karl Industries Inc., Aurora, OH and Matrix Scientific, Columbia, SC), 0.1 mM 8-bromooctanoic acid (Br8A), 0.2 mM 9-bromononanoic acid (Br9A) (Matrix Scientific), 0.2 mM 10-bromodecanoic acid (Br10A) (Matrix Scientific), 1.0 mM 11-bromoundecanoic acid (Br11A) (Fluka, St.Louis, MO), 1.0 mM 12-bromododecanoic acid (Br12A) (Fluka), 1.0 mM 15-bromopentadecanoic acid (Br15A) (Fluka), and 0.5 mM 16-bromohexadecanoic acid (Br16A). All brominated acid solutions, with the exception of Br4A, were made in 100 % ethanol. The rate and extent of formation of new MCR_{XA} complexes was measured by EPR spectroscopy (**Table 1**).

Special precautions were required for working with 4-bromobutyric acid (Br4A). This compound is unstable in neutral and alkaline solutions; therefore, all experiments were performed by dissolving it in 0.1M formic acid. Attempts to make a solution of Br4A in neutral or high pH solutions or in ethanol resulted in degradation of the acid as we inferred by a decrease in reactivity of Br4A with MCR_{red1} as a function of time.

Results

MCR_{XA} formation with brominated acids, studied by EPR and UV-visible spectroscopy

Kinetic and spectroscopic studies indicate that, when MCR_{red1} reacts with BPS, bromide is eliminated to generate a six-coordinate Ni(III)-complex with propylsulfonate as the upper axial ligand, which undergoes protonation to form propanesulfonate (17, 18, 22). This reaction is analogous to the reaction of MCR_{red1} to generate a methyl-Ni(III) intermediate in methane formation with the natural substrate, methyl-SCoM. Here we expand on a previous study to determine the range of BPS analogs that are accommodated by MCR (22). Instead of sulfonates, we used a series of commercially available brominated carboxylic acids. As described in the Introduction, we hypothesized that the reaction between MCR_{red1} and brominated acids is similar to that with BPS. To test this hypothesis, EPR and UV-visible spectroscopies were used to observe the formation of the Ni(III)-alkanoic acid complex(s), and stopped-flow experiments were conducted to characterize the kinetic parameters for the reactions. Since MCR_{XA} (alkyl-Ni(III)) and MCR_{silent} (Ni(II)) exhibit similar UV-visible spectra, unambiguous quantification of the amount of MCR_{red1} and of MCR_{XA} was performed by EPR spectroscopy by comparing the doubly integrated signal intensity with that of a Cu standard. The concentration of MCR_{silent} is then equal to the difference between the initial concentration of MCR_{red1} and the amount of MCR_{XA}. Brominated acids used in this study are abbreviated as BrXA, where X refers to total length of the chain (between 4 and 16 carbons long) including the terminal carboxyl group (A).

MCR_{red1} reacts with brominated acids that are 4 to 16 carbons in length according to Equation 1 to form MCR_{XA} (X = 4-16), which elicits an EPR signal nearly identical to that of MCR_{PS} (**Table 1**). A representative EPR spectrum of MCR_{red1} and MCR_{7A}, the product of the reaction between MCR_{red1} and Br7A, is shown in **Figure 2**.

$$MCR_{red1} + BrXA \rightarrow MCR_{XA} + Br^{-} \quad \text{Equation (1)}$$

The near identity of the EPR spectrum of the alkyl-Ni(III) MCR_{PS} state with that of MCR_{XA} strongly indicates that the reaction of MCR_{red1} with the bromoacids also generates an alkyl-Ni(III) species. The different MCR_{XA} complexes accumulate to varying amounts, as

reported in **Table 1**. Those generated from the shorter brominated acids, Br10A and below, form quickly and accumulate to fairly high amounts during a 2-min reaction at room temperature. The shortest acid tested is Br4A, which had earlier been reported to form a MCR_{PS}-like species (17, 18, 22). When reacted with MCR_{red1}, Br4A completely converts to the MCR_{4A} species; however, this reaction is unique and is discussed in more detail below. 3-Bromopropionate (Br3A) was not tested although it has been reported not to form the MCR_{XA} signal (18). Br3A is an analog of 2-bromoethanesulfonate (BES) and like BES ($[I]_{0.5\ V}$ = 2 μM), quenches the MCR_{red1} signal by the oxidation of the enzyme from Ni(I) to an EPR-silent Ni (34) state, thus BES and hence, Br3A appears to act as irreversible inhibitors of MCR (18).

The MCR_{XA} species formed from the longer (X = 11, 12, 15, and 16) brominated acids accumulate to less than 10% within 1 min at 25 °C, indicating that these complexes form transient species that form and decay more rapidly than the time it takes to hand mix and freeze the samples. When these brominated acids were reacted with MCR_{red1} at 4 °C and frozen within ~30 secs in an EPR tube, accumulation of the corresponding MCR_{XA} species markedly increased (**Table 1**). We suggest that the MCR_{XA} complexes formed with the longer brominated acids are not well anchored to the active site and, thus, escape from the radical cage and dissociate rapidly from the substrate binding channel in MCR. To better understand the reactions of MCR_{red1} with the bromoacids, stopped flow experiments were performed.

Reaction of MCR_{red1} with brominated acids and MCR_{XA} formation followed by stopped-flow

Formation of the EPR-active MCR_{XA} state is accompanied by a 35 nm red shift relative to MCR_{red1} (**Figure 3**). Exhibiting absorption maxima at 420 nm, the UV-visible absorption spectra of MCR_{XA} resemble those of MCR_{PS} (alkyl-Ni(III)), MCR_{ox1} (RS-Ni(III)), and MCR_{silent} (Ni(II)).

Stopped-flow UV-visible spectroscopy was used to obtain kinetic parameters for the reaction of MCR_{red1} with the brominated acids by monitoring the absorption bands at 385 nm and 420 nm to follow the decay of MCR_{red1} and formation of MCR_{XA}, respectively. For the reaction with each of the brominated acids, the rate constant (k) could be obtained by a single exponential equation, which adequately fit the data. The rate of decay of MCR_{red1} matches the rate of MCR_{XA} formation, which indicates that there are no intermediates in the conversion of MCR_{red1} to MCR_{XA}, or that any intermediates are too transient to be observed. These rate constants were plotted versus the BrXA concentrations to determine the second order rate constant (k_{max}/K_M) for MCR_{XA} formation as exemplified for Br7A in **Figure 4**. The second order rate constants for formation of the MCR_{XA} complexes with the shorter and medium length acids (X = 5-10) are between 20-60 $M^{-1}\ s^{-1}$ (**Table 1**, **Figures S1-S5**), with the exception of MCR_{7A}, which has a second order rate constant of 140 $M^{-1}\ s^{-1}$. The second order rate constants for formation of $MCR_{11A,}$ MCR_{12A} and MCR_{15A} (**Table 1**, **Figures S6-S8**) are significantly higher. The k_{max} and K_M values for MCR_{16A} could not be determined due to solubility issues involved with Br16A concentrations above 0.5 mM. However, with the available concentrations, a linear fit of the data established a second order rate constant of 60 $M^{-1}\ s^{-1}$ (**Table 1**, **Figure S9**).

The kinetics for formation of these MCR_{XA} complexes can be compared to those for formation of their similarly sized sulfonate cousins, MCR_{PS} and MCR_{BS}, and to the rate of methane formation from methyl-SCoM. MCR_{4A} is formed with an overall second order rate constant of 170 $M^{-1}\ s^{-1}$, which is 1000 times lower than that for formation of MCR_{PS} ($2.3 \times 10^3\ M^{-1}\ s^{-1}$ at 25 °C) (17, 18, 22). However, the k_{max} values for these reactions are nearly identical (MCR_{PS}, $17 s^{-1}$, MCR_{4A}, 15 s^{-1}); therefore, the decreased catalytic efficiency for

the formation of MCR_{4A} relative to MCR_{PS} comes exclusively from the difference in K_M values for these two substrates, ~90 mM for Br4A and ~0.09 mM for BPS. On the other hand, the k_{max}/K_M for MCR_{4A} formation is only 5.4-fold lower than the k_{cat}/K_M for methane formation from methyl-SCoM (930 M^{-1} s^{-1} at 20 °C, 1.9 × 10^4 M^{-1} s^{-1} at 65 °C) and the k_{max} value is actually 3-fold higher than the k_{cat} for methane formation at 20 °C. The second order rate constant for MCR_{5A} formation (31 $M^{-1}s^{-1}$) is 70-fold lower than that for formation of MCR_{BS} (2.3 × 10^3 $M^{-1}s^{-1}$), the analogous sulfonate complex, resulting from a 7-fold increase in K_M and a ~10-fold decrease in k_{max}. The reactions of MCR_{red1} with Br7A and Br8A exhibit kinetic parameters similar to those of the shorter bromoacids with near or complete conversion to MCR_{7A} and MCR_{8A}. For example, MCR_{7A} formation occurs with a second order rate constant of 140 M^{-1} s^{-1}, the k_{max} values are rather high (~2-3 s^{-1}) and the K_M values are similar to those of methyl-SCoM. We conclude that the short chain brominated acids are positioned in the active site much like methyl-SCoM and HSCoM and react similarly to BPS.

There is a marked drop in both k_{max} and K_M values for the reactions of MCR_{red1} with Br9A, Br10A, Br12A, Br15A and Br16A (**Table 1**, **Figures S4**, **S5** and **S7-S9**). The K_M values for most of these BrXA fall in the range of the K_M for CoBSH (~0.2 mM) (21) and the values of k_{max}/K_M for the reactions with Br11A, Br12A and Br15A are similar to the k_{cat}/K_M for CoBSH (2.2 × 10^3 $M^{-1}s^{-1}$, 20 °C) in methane formation (26), suggesting that these long chain bromoacids are recognized by MCR as CoBSH analogs. Based on a simple structural analysis using ChemDraw (**Figure 5**), the negatively charged oxygen on the carboxyl group of Br10A would be in the same position as the carboxylate oxygen of CoBSH and the oxygen from the carboxylate of Br12A would occupy the same position as the phosphate oxygen of CoBSH. The corresponding MCR_{XA} complexes decay more rapidly than those formed from the shorter BPS-like bromoacids, with <10 % of the MCR_{XA} complex accumulating when mixed at room temperature (**Table 1**). The yield of EPR-active MCR_{XA} could be increased to ~20-40 % by performing the reaction at 4 °C.

Although Br11A reacts very rapidly with MCR_{red1}, we did not observe saturation even at 60 mM concentrations; therefore, there is a relatively high standard error associated with both the K_M (200 mM) and k_{max} (380 s^{-1}) values shown in **Table 1**. The second order rate constant for MCR_{11A} formation determined from a linear fit (1500 ± 80 M^{-1} s^{-1}) is more accurate and is in reasonable agreement with that determined from a hyperbolic fit (1900 M^{-1} s^{-1}). Due to the low solubility of Br15A and Br16A, kinetic parameters were determined using brominated acid concentrations no greater than 0.5 mM. Regardless, the k_{obs}/K_M values are comparable to that obtained with Br11A; for example, for the reaction of Br15A with MCR_{red1}, the second order rate constant is 1600 $M^{-1}s^{-1}$ (**Figure S8**). Then, with Br16A, saturation could not be reached and the k_{max}/K_M value, determined from a linear fit is 57 $M^{-1}s^{-1}$.

Reaction of MCR_{red1} with Br4A - self-reactivation of MCR_{4A} to form MCR_{red}

When the reaction between MCR_{red1} and Br4A was monitored by UV-visible and EPR spectroscopy, MCR_{red1} was shown to quantitatively convert to MCR_{4A}., as shown earlier (17, 18, 22); however, when lower concentrations (~0.2 mM) of Br4A were used, a rapid decrease in absorbance at 385 nm due to formation of MCR_{4A} was observed, followed by a gradual increase in absorbance at 385 nm after ~1 min (**Figure 6**), which corresponds to the reformation of MCR_{red1}. The regeneration of MCR_{red1} occurred at either pH 10.0 or pH 7.6 in the absence of free thiols, which were shown to convert MCR_{PS} to MCR_{red1} at pH 10.0 (17, 18, 22).

The rate of MCR_{4A} generation depends on the Br4A concentration, with a second order rate constant of 170 ± 12 M^{-1} s^{-1} (k_{max}, 15 s^{-1}; K_M, 89 mM) (**Figure S10**), while the rate

constant for regeneration of MCR_{red1} (0.0067 s^{-1}) is 2200-fold slower and is independent of the Br4A concentration. At low concentrations of Br4A (i.e., 0.2 mM), there is complete (100%) conversion of MCR_{4A} to MCR_{red1} (**Figure 6**). However, at higher concentrations of Br4A, MCR_{4A} is only partially converted to MCR_{red1} and, at Br4A concentrations greater than 8 mM, there is no appreciable regeneration and the absorbance at 420 nm increases to a limiting value in a single exponential fashion. The apparent conundrum is that conversion of alkyl-Ni(III) to Ni(I) and an alkane requires a two-electron input into the Ni(III) center and no redox mediators are present; thus, it was important to determine the product of this MCR_{red1} regeneration reaction.

Mass spectrometric (MS) evidence for ester formation from the self-reactivation reaction of MCR_{4A}

Mass spectrometry was used to identify the product of the self-reactivation reaction of MCR_{red1} with Br4A (**Figure 7**). In the negative ion mode (NIM), the major peak has an *m/z* value of 250.8. This corresponds to the molecular formula $C_8H_{13}O_4Br$ with an exact mass of 252, which can be assigned to the bromo carboxy ester, 4-(4-bromobutanoyloxy)butanoic acid, $Br\text{-}(CH_2)_3\text{-}COO\text{-}(CH_2)_3\text{-}COOH$. In NIM, the loss of a proton from the carboxylic terminal group of the bromo-carboxy ester product, $Br\text{-}(CH_2)_3\text{-}COO\text{-}(CH_2)_3\text{-}COOH$, will give the expected *m/z* value of 251, i.e., (252 - 1)/1, consistent with the experimentally observed value (Inset, **Figure 7**). Confirmation that the product is the ester was obtained by MS-MS analysis of the parent ion peak (*m/z* 250.8).

Daughter ion peaks were primarily observed at *m/z* 149.5, 164.8, 171.7 (**Figure 7**). The peak at *m/z* 171.7 arises from loss of bromine from the parent ion to give $C_8H_{13}O_4$, with an exact mass of 173.2, followed by deprotonation of the carboxylic acid to give the negative ion, $[C_8H_{13}O_4]^-$, with a calculated *m/z* of 172, i.e, (252 - 79 = [173 - 1/1]=172), the fragment labeled ‘c’ in **Figure 7**. Thus, the ester can cleave at different positions marked ‘a’, ‘b’, and “c” (**Figure 7**) to form daughter ions having molecular formulae $C_4H_6O_2Br$, C_4H_6OBr and $C_8H_{13}O_4$, and the peaks marked ‘a’ and ‘b’ agree the experimentally observed *m/z* values of 164.8 and 149.5, respectively.

When the negative control experiment was performed in absence of enzyme, the product was not observed in either NIM or positive ion mode (PIM); however, a peak corresponding to the bromide was observed in NIM and the remaining fragment after de-bromination, which presumably is a positive species, was observed in PIM. Thus, the reaction of MCR_{red1} with Br4A generates the alkyl-Ni(III) species MCR_{4A}. Another molecule of Br4A reacts with MCR_{4A} to generate the ester, 4-(4-bromobutanoyloxy)butanoic acid. Two possible mechanisms by which this condensation could occur are considered in the Discussion.

MCR_{XA} is reactivated to MCR_{red1} by thiols

It has been recently observed that the MCR_{PS} complex can be reconverted to active MCR_{red1} by nucleophilic attack of various thiolates on the carbon bound to nickel. To determine if MCR_{XA} reacts similarly with thiols, we incubated the MCR_{XA} complexes with HSCoM and followed the decrease in absorbance of MCR_{XA} at 420 nm and the increase in MCR_{red1} at 385 nm (**Figure 8**). Since MCR_{XA} and MCR_{silent} have similar UV-visible spectra, we also followed the reaction by EPR spectroscopy (inset, **Figure 8**).

The rate constant for conversion of the different MCR_{XA} species to MCR_{red1} is in the range 0.003-0.012 s^{-1} (**Table 2**), which is similar to the rate constant for regeneration by HSCoM of MCR_{BS} (k_{max} of 0.006 s^{-1}) and MCR_{PS} (k_{max} is 0.011 s^{-1}). We did not observe a HSCoM concentration dependence for the rate of conversion of MCR_{XA} to MCR_{red1}; however, the

reactions with MCR_{BS} (K_M = 17 mM, **Figure S11**) and MCR_{PS} (K_M = 2.8 mM (21)) exhibit clear hyperbolic binding curves.

Among the different brominated acids shown in **Table 2**, the percent conversion of MCR_{XA} to MCR_{red1} vary, with a maximum of about 80 % conversion of MCR_{7A} to MCR_{red1} (inset, **Figure 8**). Any EPR-inactive Ni species that is formed most likely decayed into Ni(II)-MCR_{silent}. Furthermore, we did not observe conversion of MCR_{XA}, formed from the longer brominated acids (9, 10, 11, 12, 15 and 16-BrA), to MCR_{red1} when these MCR_{XA} species are incubated with HSCoM. Perhaps the MCR_{XA} complex formed from the longer acids did not reactivate because the active site may be plugged, preventing access of thiols to the active site.

Mass spectrometry evidence that a thioether product is formed from the reaction of MCR_{XA} and HSCoM

We used MS in NIM to identify the product of the reaction between MCR_{5A} and HSCoM, as CoM-S-5A, with an *m/z* value 241.3, which corresponds to the molecular formula $C_7H_{14}O_5S_2$ with an exact mass of 241.3 after loss of a proton (inset, **Figure 9**). This assignment was confirmed by MS-MS analysis of the parent ion peak at *m/z* 241.3, which yields the fragmentation pattern shown in **Figure 9**.

Daughter ion peaks were observed at *m/z* 140.9, 132.9, 107.0, 99.0 and 81.0. The daughter ion at *m/z* 132.9, labeled “b” is assigned to the 5-thiopentanoic acid fragment, with a molecular formula $C_5H_9O_2S$ in which the C-S bond is cleaved. The remaining fragment ion is desulfo-CoM with a molecular formula $C_2H_4SO_3$ and *m/z* of 107.0 (fragment labeled ‘c’). The daughter ion peak at *m/z* 140.9 (peak labeled ‘a’) corresponds to $C_2H_6O_3S_2$ with an exact mass of 141.97, which is formed when the thioether (S-C) bond is cleaved on the pentanoic acid side of the thioether group. A secondary ion that is generated from this S-C fragmentation is pentanoate, with an *m/z* of 99.0 (fragment and peak labeled ‘d’). The peak at *m/z* 81.0, labeled ‘e’, is assigned to the sulfonate group that is cleaved from various ions.

A negative control experiment performed in the absence of enzyme gave a peak at *m/z* 242.3, which is only one mass unit higher than the expected product (CoM-S-5A, *m/z* 241.3). In order to confirm if the 242.3 peak corresponds to the product, MS-MS was performed; the resulting fragmentation pattern was not consistent with that observed for CoM-S-5A product, which rules out the possibility of the thioether product in the absence of enzyme.

MS coupled with MS-MS also verified formation of the thioether products from the reactions of MCR_{6A} and MCR_{7A} with HSCoM. Thus, the MS data reveal that the reaction of HSCoM with MCR_{XA} generates a thioether product, like the reaction with MCR_{BS} and MCR_{PS}.

Discussion

We studied the reaction of MCR_{red1} with a series of brominated carboxylic acids by EPR and UV-visible spectroscopy and by kinetics. These reactions, as with BPS, apparently involve nucleophilic attack of Ni(I)-MCR_{red1} on the terminal carbon adjacent to the bromine atom to eliminate bromide and generate the EPR-active MCR_{XA} species. Compounds that give rise to the MCR_{XA} EPR signal can be abbreviated as BrXA and are generalized by the following structure: $Br\text{-}(CH_2)_{3\text{-}15}\text{-}COO^-$; where X is the alkyl linker and is ~3-15 carbons long, and A is the terminal anionic carboxylate group. Based on the near identity of the MCR_{XA} EPR signal to that of the MCR_{PS} (21), we can confidently assign MCR_{XA} as a Ni(III)-alkyl carboxylate. As with MCR_{PS}, the lack of detectable hyperfine splitting from

the bromide (I = 3/2) demonstrates that it is not near the paramagnetic center, suggesting that the bromide undergoes elimination in formation of the MCR_{XA} state.

The BrXA's were characterized by their reactivity with MCR_{red1} to form MCR_{XA} (**Table 1**), their ability to accumulate MCR_{XA} (**Table 1**), and by the rate at which the respective MCR_{XA} complexes react with thiolates ($^{-}$SCoM) to form MCR_{red1} and the CoMS-XA thioether (**Table 2**). Accumulation of MCR_{XA} (in the absence of the thiolate) is a function of the rate of MCR_{XA} formation and its decay to form XA and the EPR-silent Ni(II) MCR_{silent} state. All of these bromoacids form EPR-active MCR_{XA} species and fall into two classes, based on their reactivity (**Figure S12**).

The shorter brominated acids, Br4A to Br8A, react rapidly with MCR_{red1} to form the MCR_{XA} state, exhibit high values of K_M and k_{max} for MCR_{XA} formation, and accumulate nearly quantitatively in this state; furthermore, these compounds react with HSCoM to form a thioether and regenerate MCR_{red1}. These properties indicate that the short bromoacids mimic binding of methyl-SCoM (K_M = 5.0 mM, (31)), with their carboxylate groups interacting with Arg120.

The MCR_{4A} complex formed from the short bromoalkanoic acid, Br4A, undergoes conversion to MCR_{red1} in the absence of thiolate. One would expect Br4A to be reactive, since like BPS (the most potent inhibitor of MCR), its bromide is adjacent to an electrophilic carbon atom that is four bonds (~ 4.8 Å) from the negatively charged oxygen of the carboxylate. Accordingly, the k_{max} values for formation of MCR_{PS} and MCR_{4A} are nearly identical (~15 s^{-1}). Therefore, we propose that MCR_{red1} reacts with Br4A to form MCR_{4A}, an alkyl-Ni(III) species as with the other brominated substrate analogs. However, unlike BPS, with three oxygen atoms on the sulfonate that firmly anchor it to the active site, the carboxylate of Br4A is short of one oxygen, and thus would be held by weaker interactions (as indicated by its high K_M value). Regardless, it is likely that the alkanoate group is positioned in the active site with the methylene group bound to Ni and the carboxylate group bound to Arg120. Then, two pathways could be considered for formation of 4-(4-bromobutanoyloxy)butanoic acid, the product that is observed by mass spectrometry. In Pathway I, a second molecule of Br4A could enter the active site and nucleophilically attack the nickel-bound electrophilic carbon-4 to form the bromocarboxy ester and MCR_{red1}. The nucleophilic attack of the second Br4A is similar to the reaction of HSCoM on the MCR_{XA} species (where X = 5-8). In fact, the rate constants for formation of the thioethers and the bromocarboxy ester are similar. Another possibility, shown in pathway II, **Figure S13** is that the electrophilic methylene group bound to Ni in MCR_{4A} could undergo intramolecular attack by the negatively charged oxygen of the carboxylate to form a five-membered butyrolactone and MCR_{red1}. Then, another molecule of Br4A would react with the butyrolactone in solution or in the enzyme active site to generate the bromocarboxy ester.

The longer bromoacids, Br9A to Br16A, apparently mimic CoBSH (K_M = 0.2 mM, 21) since they bind more tightly to MCR, exhibit second-order rate constants for formation of MCR_{XA} that are similar to those for CoBSH in methane synthesis, and accumulate to a much lower extent than the shorter brominated acids. These compounds likely bind with their carboxyl group interacting with the solvent and the positively charged residues at the upper lip of the channel with the bromoalkyl chain reaching toward the nickel center, where it could react rapidly and form the MCR_{XA} complex. The unstable alkyl-Ni(III) complex then rapidly decays to an EPR silent Ni(II) state. Perhaps this is due to homolytic cleavage of the nickel carbon bond giving Ni(II)-MCR_{silent} and the corresponding alkanoic acid radical, which could abstract a hydrogen atom from the environment of protein to form the alkanoic acid (21).

Conclusion

The present studies reveal that MCR_{red1} can react with a wide range of brominated acids giving rise to an alkyl-Ni(III) complex, called MCR_{XA}, which exhibits UV-visible and EPR spectra that are nearly identical to the Ni(III)-alkylsulfonate species formed from MCR_{PS}. Thus, the MCR_{XA} complex resembles the methyl-nickel(III) species in the first step of one of the mechanisms (Mechanism I) proposed for methane formation from the natural substrates. The present studies reveal the flexibility of the active site of MCR to accommodate a broad array of substrates. The stable MCR_{XA} species (where X = 5-8) can undergo attack by nucleophilic thiols to form a thioether product and regenerate the active Ni(I) MCR_{red1} state, while MCR_{4A} converts to MCR_{red1} in the absence of a thiol. The unexpected reactivity and flexibility of the MCR active site to accommodate a broad range of substrates provides a molecular ruler for the substrate channel in MCR.

Supplementary Material

Refer to Web version on PubMed Central for supplementary material.

Acknowledgments

We thank Dr. Ashraf Raza for assistance in running mass spectrometric experiments.

This work was partly supported by a grant from the Department of Energy (SWR, DE-FG03-ER20297) and by an NSF grant (DBI-0552648) that supported Derek Lyons' research as part of a summer REU. The mass spectrometry instrumentation was purchased with funds from an NIH grant (1P20RR17675) to help support the Instrumentation Core of the Redox Biology Center at UNL.

Abbreviations

MCR	Methyl-coenzyme M reductase
methyl-SCoM	methyl-coenzyme M or, 2-(methylthio)ethanesulfonate
HSCoM	coenzyme M or, 2-thioethanesulfonate
CoBSH	coenzyme B or N-7-mercaptoheptanoylthreonine phosphate
BPS	3-bromopropane sulfonate
BBS	4-bromobutane sulfonate
MCR_{red1}	MCR exhibiting the Ni (I) EPR signal
MCR_{PS}	MCR exhibiting alkyl-Ni(III) signal arising from reaction of MCR_{red1} with BPS
MCR_{BS}	MCR exhibiting the alkyl-Ni(III) signal from the reaction of MCR_{red1} with BBS
MCR_{XA}	MCR exhibiting the alkyl-Ni(III) signal from reaction of MCR_{red1} with bromocarboxylic acids
NIM	negative ion mode

References

1. Thauer RK. Biochemistry of methanogenesis: a tribute to Marjory Stephenson. 1998 Marjory Stephenson Prize Lecture. Microbiology. 1998; 144(Pt 9):2377–406. [PubMed: 9782487]
2. DiMarco AA, Bobik TA, Wolfe RS. Unusual coenzymes of methanogenesis. Annu Rev Biochem. 1990; 59:355–94. [PubMed: 2115763]

3. Ellermann J, Kobelt A, Pfaltz A, Thauer RK. On the role of N-7-mercaptoheptanoyl-O-phospho-L-threonine (component B) in the enzymatic reduction of methyl-coenzyme M to methane. FEBS Lett. 1987; 220:358–62. [PubMed: 3111890]
4. Kruger M, Meyerdierks A, Glockner FO, Amann R, Widdel F, Kube M, Reinhardt R, Kahnt J, Bocher R, Thauer RK, Shima S. A conspicuous nickel protein in microbial mats that oxidize methane anaerobically. Nature. 2003; 426:878–81. [PubMed: 14685246]
5. Diekert G, Jaenchen R, Thauer RK. Biosynthetic evidence for a nickel tetrapyrrole structure of factor F430 from Methanobacterium thermoautotrophicum. FEBS Lett. 1980; 119:118–20. [PubMed: 7428919]
6. Diekert G, Klee B, Thauer RK. Nickel, a component of factor F430 from Methanobacterium thermoautotrophicum. Arch Microbiol. 1980; 124:103–6. [PubMed: 7377902]
7. Whitman WB, Wolfe RS. Presence of nickel in factor F430 from Methanobacterium bryantii. Biochem Biophys Res Commun. 1980; 92:1196–201. [PubMed: 7370029]
8. Ermler U, Grabarse W, Shima S, Goubeaud M, Thauer RK. Crystal structure of methyl-coenzyme M reductase: the key enzyme of biological methane formation. Science. 1997; 278:1457–62. [PubMed: 9367957]
9. Goubeaud M, Schreiner G, Thauer RK. Purified methyl-coenzyme-M reductase is activated when the enzyme-bound coenzyme F430 is reduced to the nickel(I) oxidation state by titanium(III) citrate. Eur J Biochem. 1997; 243:110–4. [PubMed: 9030728]
10. Rospert S, Bocher R, Albracht SP, Thauer RK. Methyl-coenzyme M reductase preparations with high specific activity from H2-preincubated cells of Methanobacterium thermoautotrophicum. FEBS Lett. 1991; 291:371–5. [PubMed: 1657649]
11. Craft JL, Horng YC, Ragsdale SW, Brunold TC. Nickel oxidation states of F(430) cofactor in methyl-coenzyme M reductase. J Am Chem Soc. 2004; 126:4068–9. [PubMed: 15053571]
12. Harmer J, Finazzo C, Piskorski R, Bauer C, Jaun B, Duin EC, Goenrich M, Thauer RK, Van Doorslaer S, Schweiger A. Spin density and coenzyme M coordination geometry of the ox1 form of methyl-coenzyme M reductase: a pulse EPR study. J Am Chem Soc. 2005; 127:17744–55. [PubMed: 16351103]
13. Becker DF, Ragsdale SW. Activation of methyl-SCoM reductase to high specific activity after treatment of whole cells with sodium sulfide. Biochemistry. 1998; 37:2639–47. [PubMed: 9485414]
14. Albracht SPJ, Ankel-Fuchs D, Böcher R, Ellermann J, Moll J, van der Zwann JW, Thauer RK. Five new EPR signals assigned to nickel in methyl-coenzyme M reductase from Methanobacterium thermoautotrophicum, strain Marburg. Biochimica et Biophysica Acta. 1988; 955:86–102.
15. Mahlert F, Bauer C, Jaun B, Thauer RK, Duin EC. The nickel enzyme methyl-coenzyme M reductase from methanogenic archaea: In vitro induction of the nickel-based MCR-ox EPR signals from MCR-red2. J Biol Inorg Chem. 2002; 7:500–13. [PubMed: 11941508]
16. Rospert S, Voges M, Berkessel A, Albracht SP, Thauer RK. Substrate-analogue-induced changes in the nickel-EPR spectrum of active methylcoenzyme-M reductase from Methanobacterium thermoautotrophicum. Eur J Biochem. 1992; 210:101–7. [PubMed: 1332856]
17. Hinderberger D, Piskorski RP, Goenrich M, Thauer RK, Schweiger A, Harmer J, Jaun B. A nickel-alkyl bond in an inactivated state of the enzyme catalyzing methane formation. Angew Chem Int Ed Engl. 2006; 45:3602–7. [PubMed: 16639771]
18. Goenrich M, Mahlert F, Duin EC, Bauer C, Jaun B, Thauer RK. Probing the reactivity of Ni in the active site of methyl-coenzyme M reductase with substrate analogues. J Biol Inorg Chem. 2004; 9:691–705. [PubMed: 15365904]
19. Ellermann J, Rospert S, Thauer RK, Bokranz M, Klein A, Voges M, Berkessel A. Methyl-coenzyme-M reductase from Methanobacterium thermoautotrophicum (strain Marburg). Purity, activity and novel inhibitors. Eur J Biochem. 1989; 184:63–8. [PubMed: 2506016]
20. Brenner MC, Zhang H, Scott RA. Nature of the low activity of S-methyl-coenzyme M reductase as determined by active site titrations. J Biol Chem. 1993; 268:18491–5. [PubMed: 8395504]

21. Goenrich M, Duin EC, Mahlert F, Thauer RK. Temperature dependence of methyl-coenzyme M reductase activity and of the formation of the methylcoenzyme M reductase red2 state induced by coenzyme B. J Biol Inorg Chem. 2005; 10:333–42. [PubMed: 15846525]
22. Kunz RC, Horng YC, Ragsdale SW. Spectroscopic and kinetic studies of the reaction of bromopropanesulfonate with methyl-coenzyme M reductase. J Biol Chem. 2006; 281:34663–76. [PubMed: 16966321]
23. Lahiri GK, Stolzenberg AM. Facile formation of hexahydroporphyrin complexes by reduction of octaethylisobacteriochlorinnickel(II). Angew.Chem.Int.Ed.Engl. 1993; 32:429–432.
24. Lin S-K, Jaun B. Coenzyme F430 from methanogenic bacteria: detection of a paramagnetic methylnickel(II) derivative of the pentamethyl ester by 2H-NMR spectroscopy. Helv. Chem. Acta. 1991; 74:1725–1738.
25. Lin S-K, Jaun B. Coenzyme F430 from methanogenic bacteria: mechanistic studies on the reductive cleavage of sulfonium ions catalyzed by F430 pentamethyl ester. Helv. Chem. Acta. 1992; 75:1478–1490.
26. Horng YC, Becker DF, Ragsdale SW. Mechanistic studies of methane biogenesis by methyl-coenzyme M reductase: evidence that coenzyme B participates in cleaving the C-S bond of methyl-coenzyme M. Biochemistry. 2001; 40:12875–85. [PubMed: 11669624]
27. Banerjee R, Ragsdale SW. The many faces of Vitamin-B12: Catalysis by Cobalamin dependent enzymes. Annu Rev Biochem. 2003; 72:209–247. [PubMed: 14527323]
28. Pelmenschikov V, Blomberg MR, Siegbahn PE, Crabtree RH. A mechanism from quantum chemical studies for methane formation in methanogenesis. J Am Chem Soc. 2002; 124:4039–49. [PubMed: 11942842]
29. Pelmenschikov V, Siegbahn PE. Catalysis by methyl-coenzyme M reductase: a theoretical study for heterodisulfide product formation. J Biol Inorg Chem. 2003; 8:653–62. [PubMed: 12728361]
30. Wackett LP, Honeck JF, Begley TP, Wallace V, Orme-Johnson WH, Walsh CT. Substrate analogues as mechanistic probes of methyl-S-coenzyme M reductase. Biochemistry. 1987; 26:6012–6018. [PubMed: 3120769]
31. Zehnder AJ, Wuhrmann K. Titanium (III) citrate as a nontoxic oxidation-reduction buffering system for the culture of obligate anaerobes. Science. 1976; 194:1165–6. [PubMed: 793008]
32. Schonheit P, Moll J, Thauer RK. Nickel, cobalt, and molybdenum requirement for growth of Methanobacterium thermoautotrophicum. Arch Microbiol. 1979; 123:105–7. [PubMed: 120728]

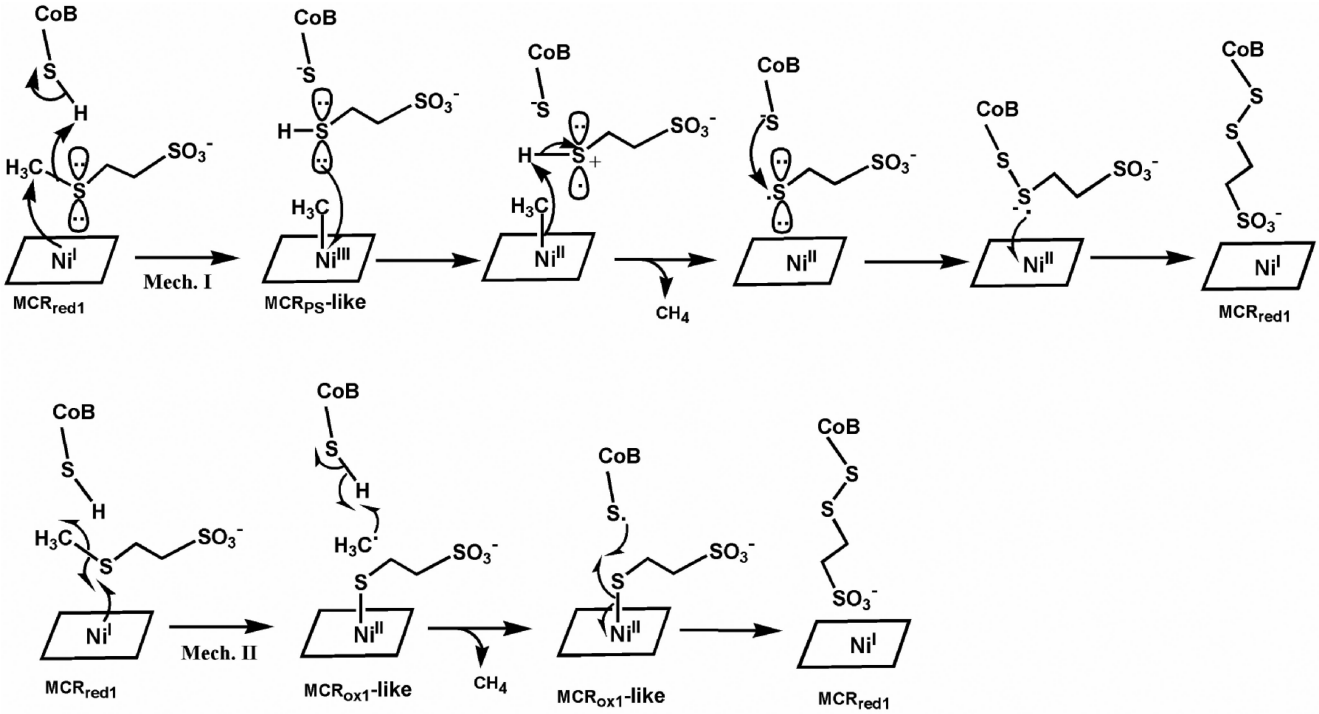

Figure 1.
Relationship between MCR_{ox1}, MCR_{PS} and the two proposed mechanisms for MCR.

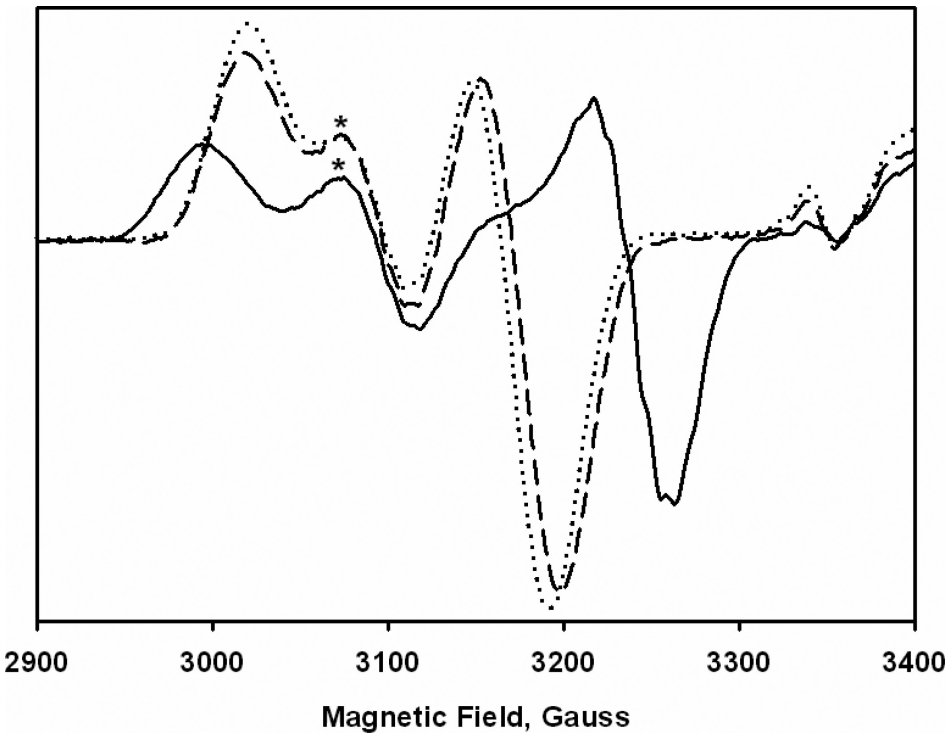

Figure 2.

EPR spectra of MCR_{7A} formed from the reaction of MCR_{red1} with Br7A. MCR_{red1} (20.6 μM (solid line)) was incubated with 1 mM Br7A (dashed line) or 548 μM BPS (dotted line) in 50 mM Tris-HCl (pH 7.6) with 0.1 mM Ti(III) citrate at 20 °C. *Contamination from MCR_{ox1}.

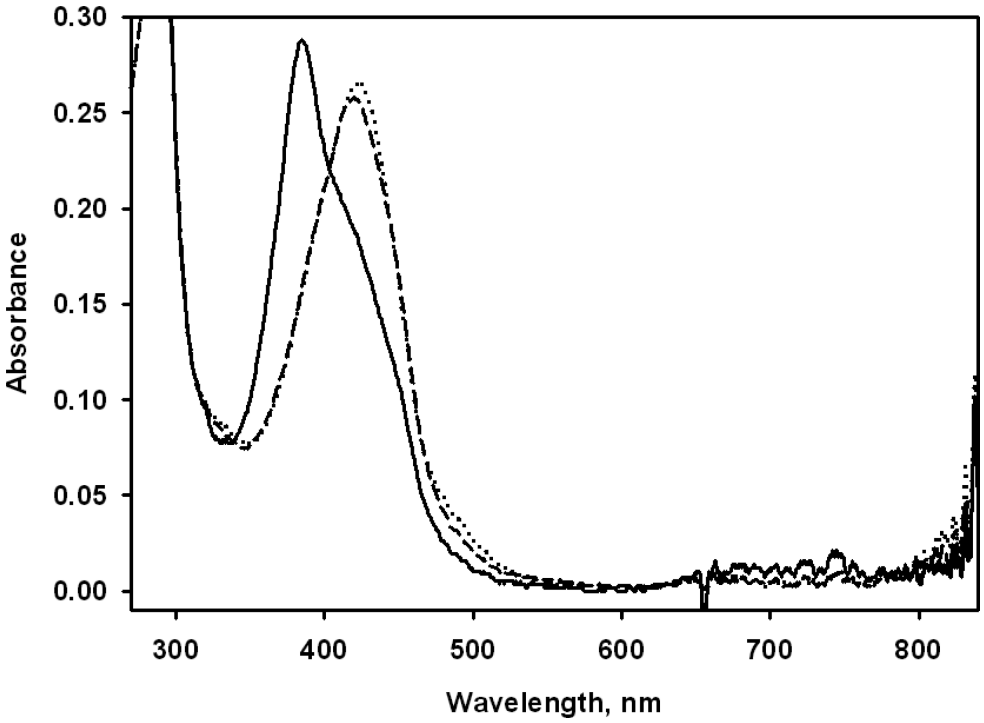

Figure 3.

UV-visible spectral changes associated with reaction of MCR_{red1} with Br7A and BPS. MCR_{red1} (8.2 μM (solid line)) was incubated with 400 μM Br7A (dashed line) or 219 μM BPS (dotted line) in 50 mM Tris-HCl (pH 7.6) with 0.1 mM Ti(III) citrate at 20 °C.

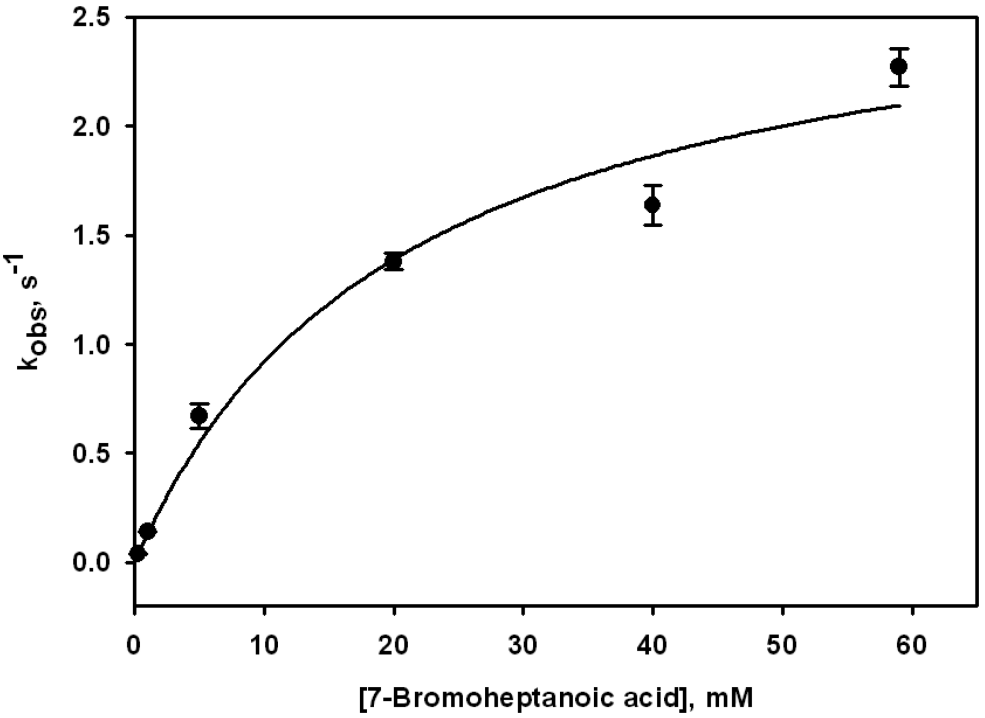

Figure 4.

Dependence of k_{obs} for MCR_{7A} on Br7A concentration. 10 μM MCR_{red1} was converted to MCR_{7A} by the addition of different concentrations of Br7A in 0.5 M Tris-HCl, pH 7.6 containing 0.2 mM Ti(III) citrate. The data were fit to a 2-parameter hyperbolic equation with a k_{max} of 2.8 ± 0.4 s^{-1} and K_M of 21 ± 8 mM and a second order rate constant of 140 ± 57 M^{-1} s^{-1}.

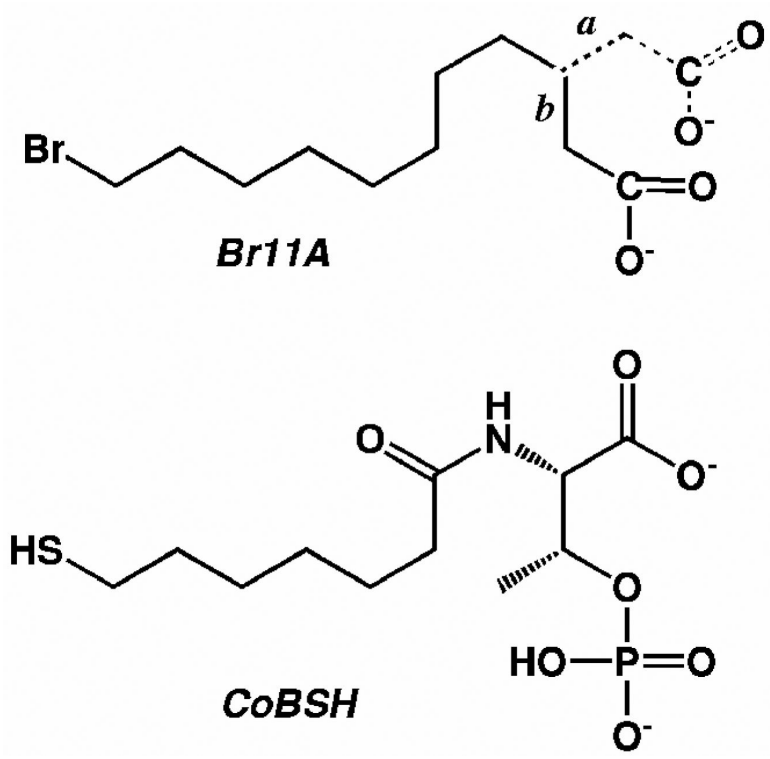

Figure 5.
Comparison of the structures of Br11A and CoBSH. Two alternative conformations (a and b) are shown by the solid and dotted lines.

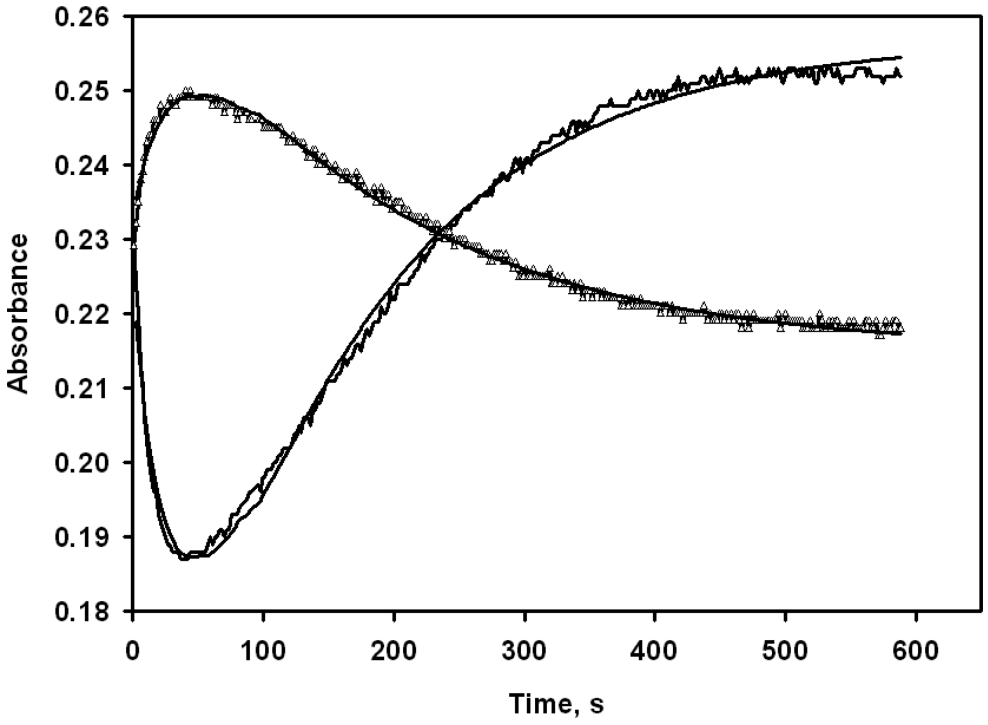

Figure 6.

Formation of MCR_{4A} followed by regeneration of MCR_{red1}. The formation or decay of MCR_{4A} and MCR_{red1} were monitored at 385 nm (solid line) and 420 nm (open triangles) by UV-visible spectroscopy. MCR_{red1} (10 μM) was reacted with 0.2 mM Br4A in 200 mM ammonium carbonate, pH ~ 10. The data were fit to three-component sequential equations with the following parameters: for the absorbance changes at 385: k_1, 0.037 ± 0.003 s^{-1}; k_2 = 0.0067 ± 0.0003 s^{-1}; for the absorption changes at 420 nm: k_1, 0.036 ± 0.001 0 s^{-1}, k_2 0.0054 ± 0.0007 s^{-1}.

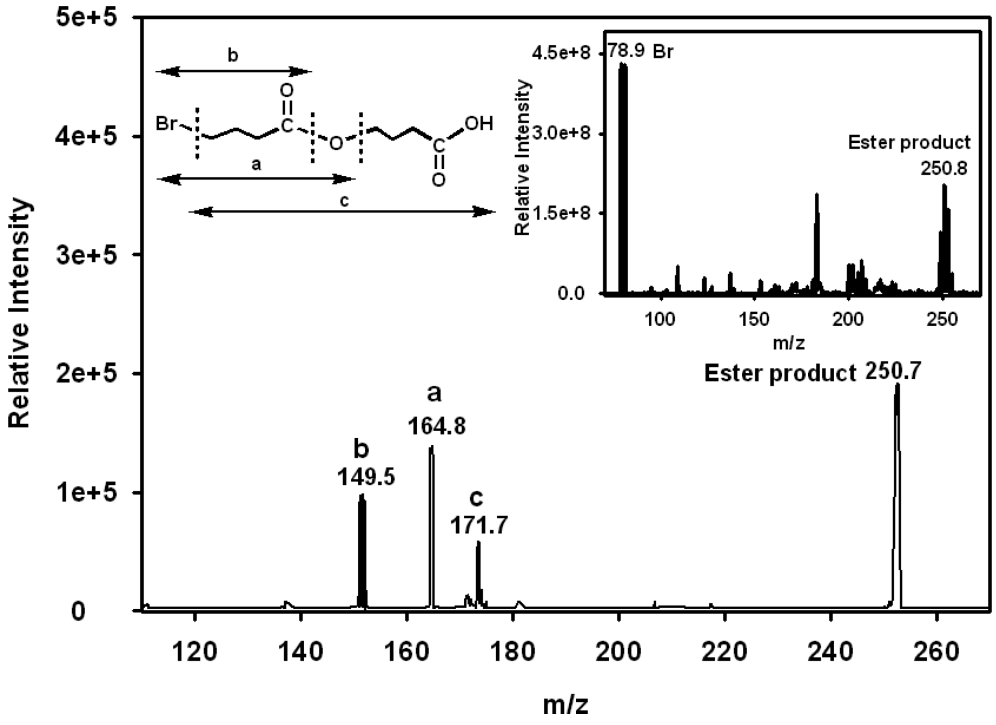

Figure 7.

NIM MS-MS identification of the fragmented/daughter ions from the bromocarboxy ester product formed from the "self-reactivation" of MCR_{4A} to MCR_{red1}. MCR_{red1} (10 μM) was reacted with 2.0 mM Br4A in 20 mM ammonium carbonate, pH ~ 10. Inset: NIM ES-MS identification of the bromo-carboxy ester product formed from the "self-reactivation" of MCR_{4A} to MCR_{red1}.

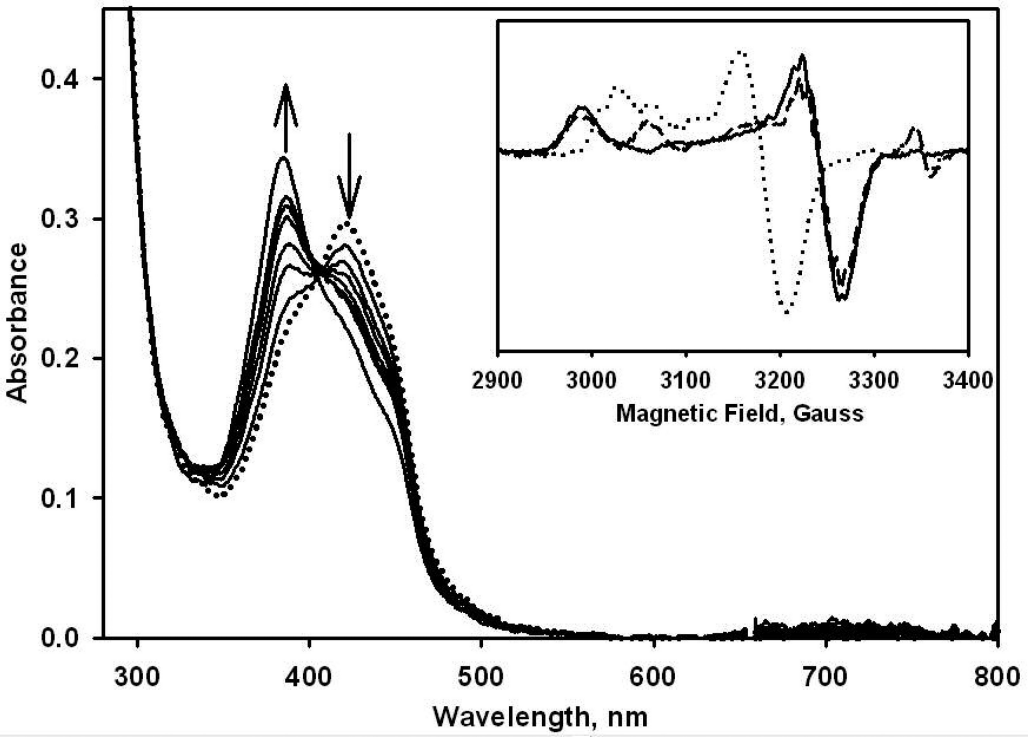

Figure 8.

UV-visible spectral changes associated with the regeneration of MCR_{red1} from MCR_{7A} incubated with 20 mM HSCoM. MCR_{red1} (11.52 μM (solid line)) was treated with 100 μM Br7A (dotted line) and the MCR_{7A} formed was incubated with 20 mM HSCoM in 1M TAPS-Na (pH ~ 10) at 20 °C and the absorbance was recorded every 6 mins for over 40 mins. Inset: Representative EPR spectra of MCR_{red1} (solid line) MCR_{7A} (dotted line) and regeneration of MCR_{7A} to MCR_{red1} (dashed line).

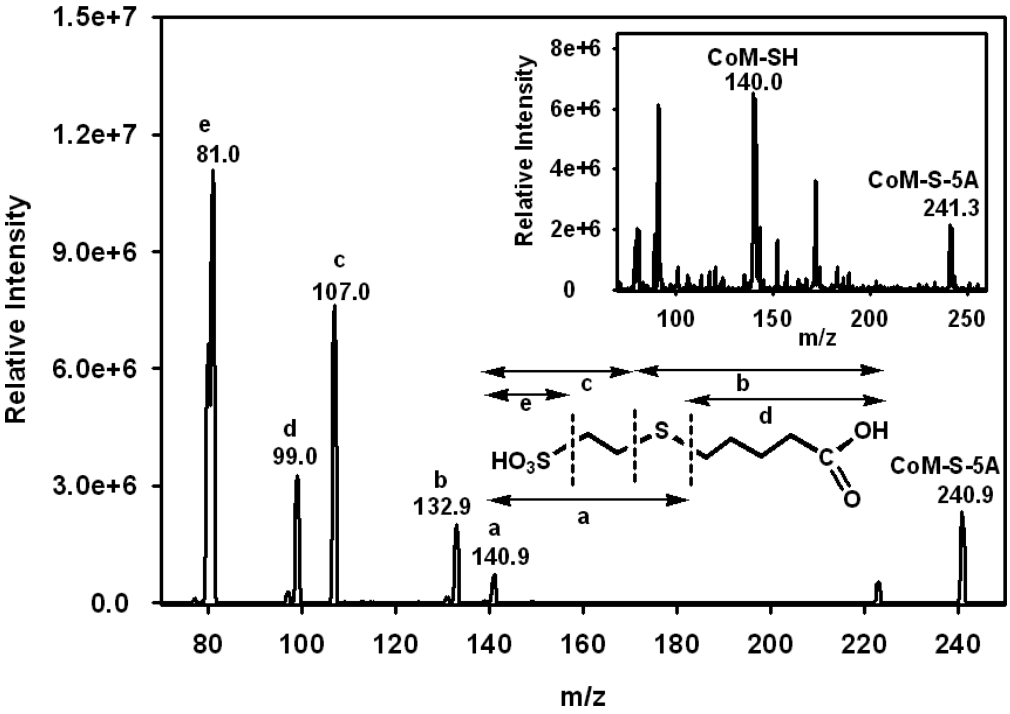

Figure 9.

NIM-MS/MS spectrum of the product of the reaction of MCR_{5A} with HSCoM. 20 μM MCR_{red1} was reacted with 1mM Br5A to form MCR_{5A}, which was reacted with 1 mM HSCoM in 500 mM ammonium carbonate pH ~ 10.0. Inset: Original NIM-MS spectrum of the reaction product.

Table 1

Kinetic parameters for the conversion of MCR_{red1} to MCR_{XA}.

Chemical Name	Chemical Structure	$MCR_{red1} \rightarrow MCR_{XA}$ (% Conversion)[c]	k_{max} (s^{-1})	K_M (mM)	k_{max}/K_M (M^{-1} s^{-1})[a]
Br4A	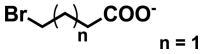 n = 1	85 ± 15	15 ± 0.6	88 ± 5	170 ± 12
Br5A	n = 2	56 ± 10	2.0 ± 0.5	65 ± 27	31 ± 15
Br6A	n = 3	53 ± 10	0.27 ± 0.05	5.2 ± 3.6	53 ± 38
Br7A	n = 4	93 ± 7	2.2 ± 0.3	21 ± 7	140 ± 57
Br8A	n = 5	93 ± 1	2.1 ± 0.5	92 ± 34	23 ± 10
Br9A	n = 6	60 ± 2	0.074 ± 0.003	1.3 ± 0.2	56 ± 7
Br10A	n = 7	12 ± 8	0.050 ± 0.002	2.2 ± 0.5	22 ± 2
Br11A	n = 8	<5 (13 ± 5)	380 ± 170	200 ± 110	1900 ± 1300 1500 ± 80[b]
Br12A	n = 9	<5 (10 ± 5)	0.28 ± 0.02	0.93 ± 0.26	500 ± 92
Br15A	n = 12	6 (20 ± 5)	0.26 ± 0.04	0.16 ± 0.11	1600 ± 1000 470 ± 64[b]
Br16A	n = 13	8 (41 ± 2)	ND	ND	57 ± 18[b]

[a] Second-order rate constants were determined by a hyperbolic fit.

[b] Second-order rate constants determined by fitting data to a linear equation.

[c] The % conversion was determined by EPR. The number in the parenthesis was obtained when the reaction was performed on ice. For details, refer to experimental section

Table 2

Regeneration of MCR_{red1} from MCR_{XA} using 20 mM HSCoM. Experiments were performed in 0.5 M TAPS (pH 10) at 25 ^{o}C.

Chemical Name	Reactivation of MCR_{XA}	$MCR_{XA} \rightarrow MCR_{red1}$ (% reactivation)[a]	k_{obs} (s^{-1})
Br5A	Yes	46	0.012 + 0.001
Br6A	Yes	65	0.006 ± 0.001
Br7A	Yes	81	0.006 ± 0.001
Br8A	Yes	31	0.003 ± 0.001
Br9A	No	Negligible	NA

[a]The % reactivation represents the percentage conversion of MCR_{XA} to MCR_{red1}. For details of experimental conditions, refer to experimental section.